

CAUGHT IN FORMATION: THE NUCLEAR-CLUSTER-TO-BE IN NGC 2139 \*

DAVID R. ANDERSEN<sup>1</sup>, C. JAKOB WALCHER<sup>2,3</sup>, TORSTEN BÖKER<sup>4</sup>, LUIS C. HO<sup>5</sup>, ROELAND P. VAN DER MAREL<sup>6</sup>,  
HANS-WALTER RIX<sup>7</sup>, JOSEPH C. SHIELDS<sup>8</sup>

<sup>1</sup>NRC Herzberg Institute of Astrophysics, 5071 West Saanich Road, Victoria, BC, V9E 2E7, Canada,

<sup>2</sup>Observatoire Astronomique de Marseille Provence, Traverse du Siphon, 13376 Marseille Cedex 12, France,

<sup>3</sup>Institut d'Astrophysique de Paris, 98bis, Boulevard Arago, 75014 Paris, France,

<sup>4</sup>ESA/ESTEC, Keplerlaan 1, 2200 AG Noordwijk, Netherlands,

<sup>5</sup>The Observatories of the Carnegie Institution of Washington, 813 Santa Barbara Street, Pasadena, CA 91101-1292, USA,

<sup>6</sup>Space Telescope Science Institute, 3700 San Martin Drive, Baltimore, MD 21218, USA,

<sup>7</sup>Max Planck Institut für Astronomie, Königstuhl 17, 69117 Heidelberg, Germany,

<sup>8</sup>Department of Physics and Astronomy, Clipping Research Laboratories 251, Ohio University, Athens, OH45701-2979, USA

*Draft version October 31, 2018*

ABSTRACT

Close to its center, the bulgeless galaxy NGC 2139 hosts a star cluster that is younger and less massive than any actual nuclear star cluster (NC) studied so far. We have measured the H $\alpha$  velocity field around the photometric center of this galaxy using the VLT ARGUS integral field unit and GIRAFFE spectrograph in order to constrain different proposed theories of NC formation. We observe that the best-fit kinematic center and the candidate NC appear to be separated by 2.8'' (320 pc). Indeed, the kinematic center also is offset from the galaxy's photometric center and a possible bar or extended region of star formation in which the young cluster resides, implying that this galaxy is not in dynamic equilibrium. The H $\alpha$  flux map also reveals other regions of strong star formation in the possible bar. These observations suggest that a nascent NC is forming away from the kinematic center of NGC 2139 which may come to rest there on a time scale of a few 100 Myr.

*Subject headings:* galaxies: nuclei — galaxies: star clusters — galaxies: individual (NGC 2139)

1. INTRODUCTION

Galaxy centers continue to attract special interest as they host a number of distinctive phenomena, such as active galactic nuclei, central starbursts and extremely high stellar densities. The last decade has shown that the evolution of galaxies is closely linked to the evolution of their nuclei, as evidenced by a number of relations between global and nuclear properties (e.g. Magorrian et al. 1998; Ferrarese & Merrit 2000; Gebhardt et al. 2000; Graham et al. 2001; Ferrarese 2002; Häring & Rix 2004).

In view of this general paradigm and as a contribution to the full census of galaxy nuclei over all Hubble types, we are studying the central region of late-type, bulgeless spirals. Prime candidates for the nuclei of bulgeless spirals have been identified in the form of “nuclear star clusters” (NCs). Such compact, photometrically distinct NCs are found in, or very near, the centers of spirals across all Hubble types (Phillips et al. 1996; Carollo, Stiavelli & Mack 1998; Böker et al. 1999; Matthews et al. 1999; Böker et al. 2002, Balcells et al. 2003, Scarlata et al. 2004), as well as ellipticals (see e.g. Côté et al. 2006 and references therein).

Due to the lower surface brightness of the background galaxy, NCs in bulgeless galaxies can be studied in more detail than those in earlier Hubble types. It has been shown that NCs in bulgeless galaxies have a number of unusual properties: they often are the most luminous

cluster of their host galaxy and they lie inside the error-bars assigned to the location of the photometric center (Böker et al. 2002). Although they are as compact as globular clusters (Böker et al. 2004), they are one order of magnitude more massive than the massive end of the Galactic globular cluster mass function (Walcher et al. 2005). They also show evident signs of repetitive star formation (Walcher et al. 2006), which may lead to the formation of disks that are photometrically distinct (bluer) from the underlying NC (Seth et al. 2006). Finally, there are two examples of AGNs hosting NCs: NGC 4395 (Fillipenko & Ho, 2003) and NGC 1042 (Shields et al. 2008). There also is evidence that the mass of the NC correlates with the mass of its host galaxy (Rossa et al. 2006). NCs are thus prime candidates for representing the unique centers of otherwise bulgeless galaxies.

At least three different scenarios for the formation (and evolution) of NCs can account for most of their properties.

(1) NC formation may be a generic property of late-type spirals, if the dynamical center of the galaxy is an a priori well-defined location. This would e.g. be the natural consequence of a dark matter halo with a cuspy density profile. Magneto-rotational instability could then produce a steady gas inflow onto the galaxy center (Milosavljević 2004). Recently, compression of gas through tidal forces has also been suggested as a possible formation route for NCs (Emsellem & van der Ven, 2008). An observational signature of this scenario would be the coincidence of the NC location with the location of the kinematic center as well as a rather ordered velocity field.

(2) On the other hand NC formation could be a ran-

\*BASED ON OBSERVATIONS COLLECTED AT THE EUROPEAN SOUTHERN OBSERVATORY, CHILE, PROPOSAL NO. 74.B-0264

Electronic address: david.andersen@nrc-cnrc.gc.ca

dom process. In this picture, any randomly formed, “free-roaming” seed cluster close to the overall center of a bulgeless galaxy would accumulate further gas in the gas-rich central region. The deeper potential well of the cluster then induces star formation in the accreted gas, thus leading to the very compact, massive objects we observe. The velocity fields would not necessarily be centered on the NC or be well-ordered. This scenario would be expected, if the central potential of bulgeless galaxies were similar to the constant density cores advocated by some in the literature (see e.g. de Blok, Bosma & McGaugh, 2003 and references therein).

(3) Finally, objects broadly similar to NCs could coalesce through the merging of several young clusters formed close to each other in a starburst event (Oh & Lin 2000; Fellhauer et al. 2002; Capuzzo-Delcetta & Miocchi 2008).

However, by construction, the distinction between the three formation mechanisms will be blurred with time. In either the second or third formation mechanisms, the formed cluster is drawn to the center of the potential well by dynamical friction. For the case of a deep central potential, the dynamical friction timescale (Chandrasekhar 1943) for a proto-NC can be estimated from Equation (3) of Milosavljević (2004), which gives a lower bound for the decay timescale  $t_{\text{decay}}$  with which a cluster would sink to the kinematic center of the galaxy:

$$t_{\text{decay}} \gtrsim 3 \times 10^7 \text{yr} \left( \frac{v_{\text{circ}}}{50 \text{ km s}^{-1}} \right) \left( \frac{r}{100 \text{ pc}} \right)^2 \left( \frac{M_{\text{cl}}}{10^6 M_{\odot}} \right)^{-1}, \quad (1)$$

where  $v_{\text{circ}}$  is the velocity of the cluster on an assumed circular orbit,  $r$  is the radius of that orbit and  $M_{\text{cl}}$  is the mass of the cluster. This decay timescale can be quite short, after which all three scenarios follow the same evolutionary path, where a massive pre-existing cluster soaks up any infalling gas.

Distinguishing between the three scenarios quoted above is not only central to the identification and formation of NCs, it also helps inform the debate over the form of the central potential of low surface brightness galaxies (e.g. de Blok 2005 and Valenzuela et al. 2007). If scenario 1) could be shown to be valid, this would strongly support the theory predicting diverging mass profiles in bulgeless disc galaxies. Scenarios 2) or 3) would be unlikely if the environment close to the NC were influenced by a steep gravitational potential.

Observational signatures of any of the three NC formation mechanisms described above will most easily be found in galaxies with a young NC. In particular, the velocity field around a NC is interesting, as it allows us to search for a possible offset between the kinematic center and the NC. Such an offset would allow to clearly distinguish between the different formation scenarios. To maximize the chances of finding a NC offset from the kinematic center, one would ideally target a galaxy whose photometric center were offset from its NC. In NGC 2139, we have a galaxy that meets these criteria: NGC 2139 contains a candidate NC that is somewhat offset from the photometric center and is very young as compared to other NCs. This candidate NC is also less massive than any other NC whose mass has been measured.

After introducing the properties of NGC 2139 and its

central cluster, we present the H $\alpha$  emission line velocity field of NGC 2139 measured using the ARGUS integral field unit (IFU) of ESO’s Very Large Telescope (VLT), focusing on the innermost region directly around the potential nucleus of the galaxy. Finally, we evaluate our results both in terms of the NC formation scenarios described above and in terms of the possibility that the central cluster of NGC 2139 is actually a very young super star cluster (SSC) similar to those found in some starburst galaxies which may over time fade from view and not become a galaxy proto-nucleus.

## 2. PREVIOUS OBSERVATIONS OF NGC 2139

NGC 2139 is morphologically classified as an SABcd galaxy (de Vaucouleurs et al. 1991, RC3). It is one of the 1000 brightest galaxies in the HIPASS survey (Koribalski et al. 2004), and has a recession velocity of 1837 km/s and a HI velocity width of  $W_{50} = 206.7$  km/s. Based on its velocity width, it is expected to have a maximum, projected rotation velocity of 94 km/s (Paturel et al. 2003). However, the HI profile available from the HIPASS archive is quite asymmetric with the primary peak having a velocity of  $\sim 1785$  km/s. A survey of spatially resolved 1.425 GHz emission from IRAS bright galaxies (Condon et al. 1996) indicates that the radio emission from NGC 2139 comes from two components: a primary lobe associated with the main body of the galaxy and a secondary lobe associated with the plume extending south of the galaxy. The large-scale morphology as seen from publicly available Digitized Sky Survey (DSS)<sup>1</sup> images is irregular showing a few pronounced spiral arms and some tidal features. This, along with many HII-region candidates concentrated near the center, are evidence for strong star formation and a possible recent merger event. The HST WFPC2 F814W image (Böker et al. 2002) clearly shows a luminous band (again presumably star-forming) going through the center of the galaxy, indicating a possible bar or star formation filament triggered through gas inflow to the center of the galaxy. This band also includes the luminous star cluster that Böker et al. (2002) classified as a NC.

This central star cluster is unique in several ways. It is the youngest ( $4.1 \times 10^7$  yr) star cluster in a sample of nine NCs studied in Walcher et al. (2006, see also Rossa et al. 2006). From an in-depth analysis of its spectrum these authors find that the spectrum is actually consistent with the cluster not containing any old stellar population whatsoever. It also is the least massive in their sample (Walcher et al. 2005), with a dynamically determined mass of just  $M_{\text{cl}} = 8.3 \times 10^5 M_{\odot}$ . We note that this star cluster is probably less massive than most NCs, as Rossa et al. (2006) find from a much larger sample with masses derived from stellar population analysis that the inability to infer spectroscopically the populations of faint clusters does introduce a bias towards younger ages, but not necessarily towards higher masses. It is also noteworthy in this context that the effective radius

<sup>1</sup> The Digitized Sky Surveys were produced at the Space Telescope Science Institute under U.S. Government grant NAG W-2166. The images of these surveys are based on photographic data obtained using the Oschin Schmidt Telescope on Palomar Mountain and the UK Schmidt Telescope. The plates were processed into the present compressed digital form with the permission of these institutions.

of the NGC 2139 central cluster is 10pc, making it one of the largest in the Boeker et al. (2004) sample.

Indeed, as Walcher et al. (2005) posit, the central cluster in NGC 2139 may be a forming NC, thereby providing an excellent chance to identify an example for scenario 2). Because the fate of the NGC 2139 cluster is still unknown, we will use the term “central cluster” (*not* NC) for the remainder of this paper, in order to avoid confusion with bona-fide NCs that (already) occupy the kinematic center of their host galaxy.

### 3. DATA AND REDUCTIONS

Observations of NGC 2139 were carried out with the ARGUS integral field unit (IFU) coupled to the GIRAFFE spectrograph on the Kueyen telescope of ESO’s Very Large Telescope (VLT) in May of 2004. We used the 0.52” lenselet scale-size, i.e. a field of view of 11.5” by 7.3”, and the LR06 grating which yields a resolution of  $R \approx 13700$  covering a wavelength range from  $6400\text{\AA} < \lambda < 7100\text{\AA}$ . The seeing during the observations was reported to be 0.8”. Because the goal of the observations was simply to study the velocity field, no flux calibration was performed.

Data were overscan- and bias-corrected and trimmed using the NOAO *IRAF*<sup>2</sup> package *ccdproc*. Cosmic ray rejection was performed before spectral extraction using a method described in Andersen et al. (2006). Following cosmic-ray cleaning, basic spectral extraction, flattening, wavelength calibration and sky subtraction were done using *IRAF dohydra*. Extracted one-dimensional spectra were field-flattened with dome flats and wavelength-calibrated using ThAr emission spectra. Finally, the 14 sky spectra were averaged and the mean sky spectrum was subtracted from the 299 source spectra.

Once spectra were processed, we identified H $\alpha$  emission-lines and measured Gaussian fluxes, widths, centers and the corresponding errors for lines in a 20 $\text{\AA}$  spectral window around the redshifted H $\alpha$  line. We detected H $\alpha$  emission in 298 of 299 object spectra. Most H $\alpha$  emission-lines of NGC 2139 required multiple Gaussian lines to be fit. We modified the algorithm used in Andersen et al. (2006) in order to incorporate two Gaussian profiles in the Marquardt–Levinson fit. Errors on line centroids were obtained from the covariance matrix. We fit all H $\alpha$  spectra with both one and two Gaussian profiles. We compared the reduced  $\chi^2$  ( $\chi^2_\nu = \chi^2/(n-p)$ , where  $n$  is the number of data points and  $p$  is the number of free parameters) values of both fits. Spectra with a  $\chi^2_\nu$  ratio less than 1.1 were classified as single lines (type 1), while all others were classified as having two components. Of the 298 detected H $\alpha$  emission lines, 278 were better fit with two Gaussian lines. Using a visual inspection, we classified the multiple line fits in three categories (Figure 1): single narrow lines with wide wings (type 2); single narrow lines with wide wings that are offset from the central peak (type 3); and finally two kinematically distinct features (type 4). We find that only 88 of the 278 lines are best fit by two Gaussian profiles and belong to the last category type 4 with two unique components.

<sup>2</sup> IRAF is distributed by the National Optical Astronomy Observatories, which are operated by the Association of Universities for Research in Astronomy, Inc., under cooperative agreement with the National Science Foundation.

With this information, the kinematics of NGC 2139 can be divided into two components. To extract the measures of widths and centroids for component A, we used the single Gaussian for type 1 spaxels and the properties of the more highly peaked Gaussian for type 2, 3 and 4. For the flux in the line we used the flux in the core and the wings, when present, for types 1, 2 and 3, while we used the flux in the main component only for type 4 spaxels. For the second component, called B, we used the properties of the secondary H $\alpha$  emission peak when unambiguously present (type 4).

The first component (A) shows clear rotation in the velocity field (Figure 2). No structure in the width of this component is apparent, while it shows two distinct peaks in flux. On the other hand, the second component (B; Figure 3) does not rotate, clearly has a larger dispersion in line widths and has no clearly discernible peak in flux. Physically speaking, we have attempted to separate a disc-motion component A from a random-motion component B. In almost all of the cases the widths of the narrow component A is around  $\sigma \sim 15$  km/s and that of the broad component B is  $\sigma > 50$  km/s. That and the regularity of component A and the irregularity of component B support our interpretation as disc and random-motion component, respectively.

### 4. ANALYSIS

#### 4.1. Velocity Field Modeling

We used the centroids of the narrow component A described above as the input to our velocity field modeling. Our velocity field model incorporates two simplifying assumptions: the rotation of the gas in the disk is circular and the shape of the rotation curve can be approximated by a tanh function [ $V_{\text{mod}}(R, \theta) = V_{\text{sys}} + V_{\text{rot}} \tanh(R/h_{\text{rot}}) \cos \theta$ ; Andersen et al. 2001]. Keeping these assumptions in mind, we are in general able to solve for a number of disk parameters, including 1) the kinematic center, 2) the major axis position angle, 3) the systemic velocity,  $V_{\text{sys}}$ , 4) a rotation velocity,  $V_{\text{rot}}$ , and scale length,  $h_{\text{rot}}$ , which match the velocity field over the ARGUS field. The best fit and covariance matrix were determined by minimizing  $\chi^2$  using a modified Levenberg-Marquardt algorithm.

One can compare an IFU spaxel to a radio beam; both smooth or “smear” signal velocities within either the spaxel or the radio beam. We accounted for the effect of beam smearing by mapping the model over the region spanned by the observations on a grid with a scale of 10 “pixels” per spaxel (0.052”). By determining the standard deviations of velocities within each spaxel and incorporating this error in our calculation of  $\chi^2$  we are, in effect, applying a beam-smearing correction.

Our best fits to the velocity field yielded small velocity-field residuals (Figure 4), with standard deviations of just  $\sim 7$  km/s, but our velocity centroiding errors were even smaller, resulting in minimum reduced- $\chi^2$ ,  $\chi^2_\nu$ , for these fits which were typically much greater than unity ( $\chi^2_\nu \approx 50$ ). For any fit where  $\chi^2_\nu$  is much greater than unity there are several possible explanations: (1) the residuals of our velocity field model fit are not Gaussian, (2) error-bars on the line centroids are underestimated, or (3) the model is not a good representation of the data. Indeed, one would not expect our simple model to approximate

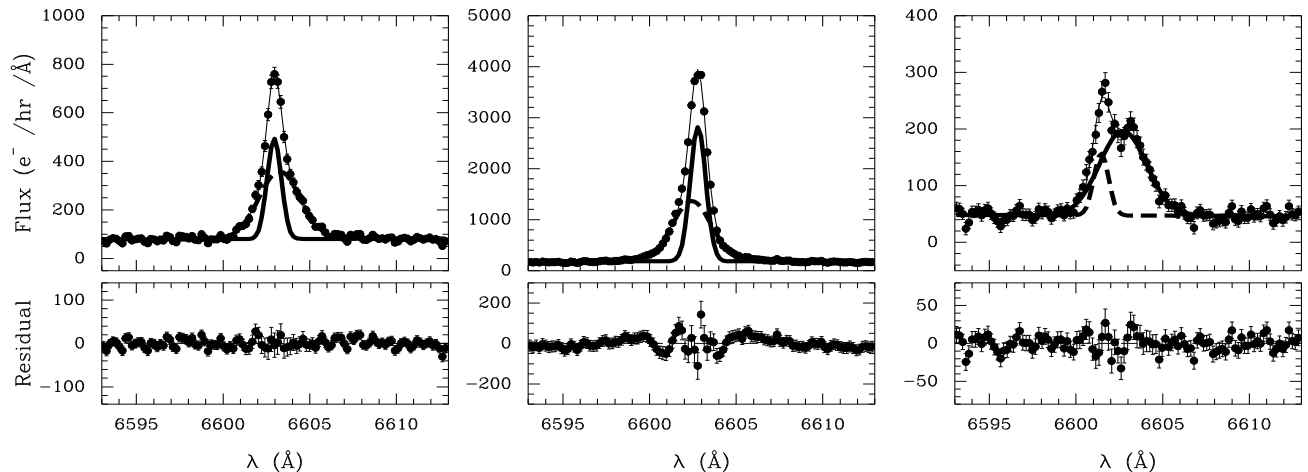


FIG. 1.— The H $\alpha$  emission lines from three ARGUS IFU spaxels with the best double-Gaussian fits (top) and fit residuals (bottom). H $\alpha$  was detected in 298/299 spaxels, but most line profiles cannot be well-fit by a single Gaussian. Rather, almost all (278/298) line profiles are better fit with a double Gaussian profile. In the two panels towards the left, one component appears to be stronger and have a narrower width while the other component fits the broad wings. The leftmost panel is an example of a type (2) profile identified in the text. The central panel shows a type (3) profile in which the broad wings are offset from the narrower peak. On the right is an example of a line with two clear kinematic components (type 4, as identified in the text). This latter phenomenon was detected in 88/298 ARGUS spectra.

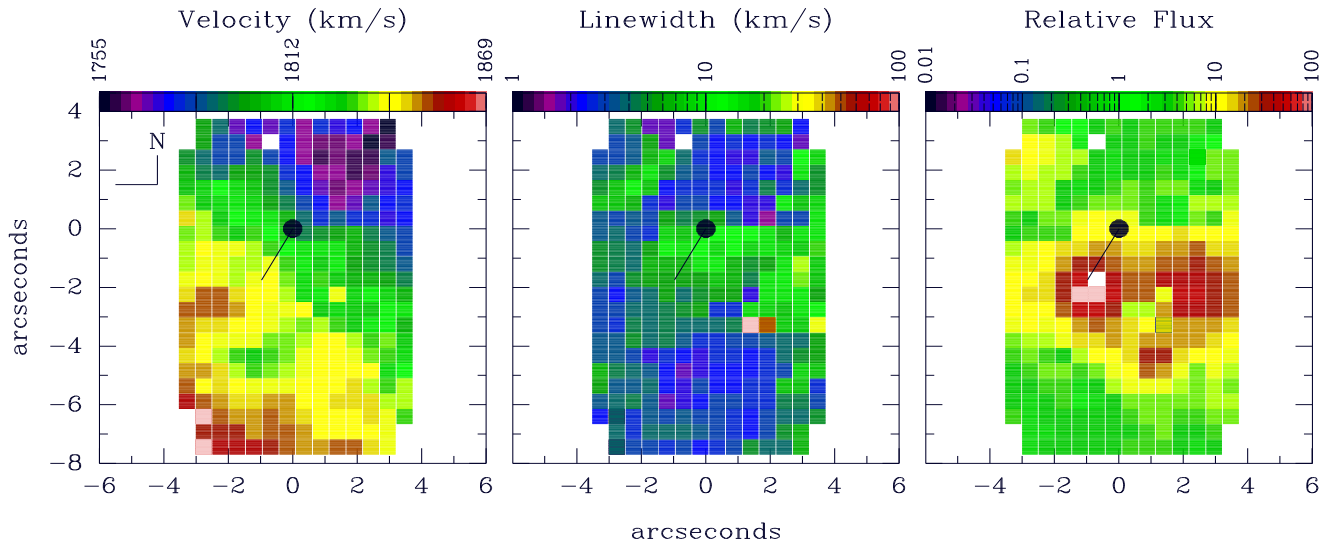


FIG. 2.— Velocities (left), widths (center) and fluxes (right) of the narrow line profile component (component A). Rotation is clearly apparent in the velocity field and a simple model fits the velocity measurements adequately. The location of the best-fit kinematic center is marked with a filled circle. The line from the point marks the direction of the kinematic major axis. Approximately 5'' South of the kinematic center is a significant kinematic asymmetry. We find nothing remarkable in the width field, perhaps just a slight broadening of the H $\alpha$  line roughly coincident with the kinematic center. Two peaks in the flux distribution are clearly visible, but as we show in Section 4.2, neither peak corresponds to the locations of the central cluster or the kinematic asymmetry.

the true velocity field because in detail the velocity fields of real galaxies can be complicated on fine spatial scales. Since the spectral and spatial resolution of our ARGUS observations is relatively high, it is reasonable to suppose we are seeing the true complexities of the kinematics at the center of NGC 2139. Presumably a class of models exists which would better match the data, but would become increasingly complex.

Since we are not interested here in modeling the random motions of HII regions and the non-random, high spatial frequency streaming associated with spiral arms or other similar features, we assumed these variations have a random spatial distribution. We compensated for these contributions by adding a “fuzziness” term to our model. Specifically, we follow the probability theory ar-

guments of Rix et al. (1997) and add an extra error term,  $\sigma_{\text{mod}}$ , into the  $\chi^2$  sum (which we denote as  $\chi_{\delta}^2$  to differentiate it from the usual definition of  $\chi^2$ ):

$$\chi_{\delta}^2 = \sum_i \frac{(V_{\text{mod}_i} - V_{\text{obs}_i})^2}{\sigma_{\text{mod}}^2 + \sigma_{\text{obs}_i}^2}, \quad (2)$$

where  $V_{\text{mod}_i}$  is the model velocity at the location of the  $i^{\text{th}}$  spatial element,  $V_{\text{obs}_i}$  is the observed velocity of the  $i^{\text{th}}$  spatial element, and  $\sigma_{\text{obs}_i}$  is the standard deviation on  $V_{\text{obs}_i}$ , including both the effects of beam-smearing and the centroid measurement error.

Using our model, we were not able to find a unique solution for the disk inclination of NGC 2139, but we were able to find unique solutions by fixing the inclina-

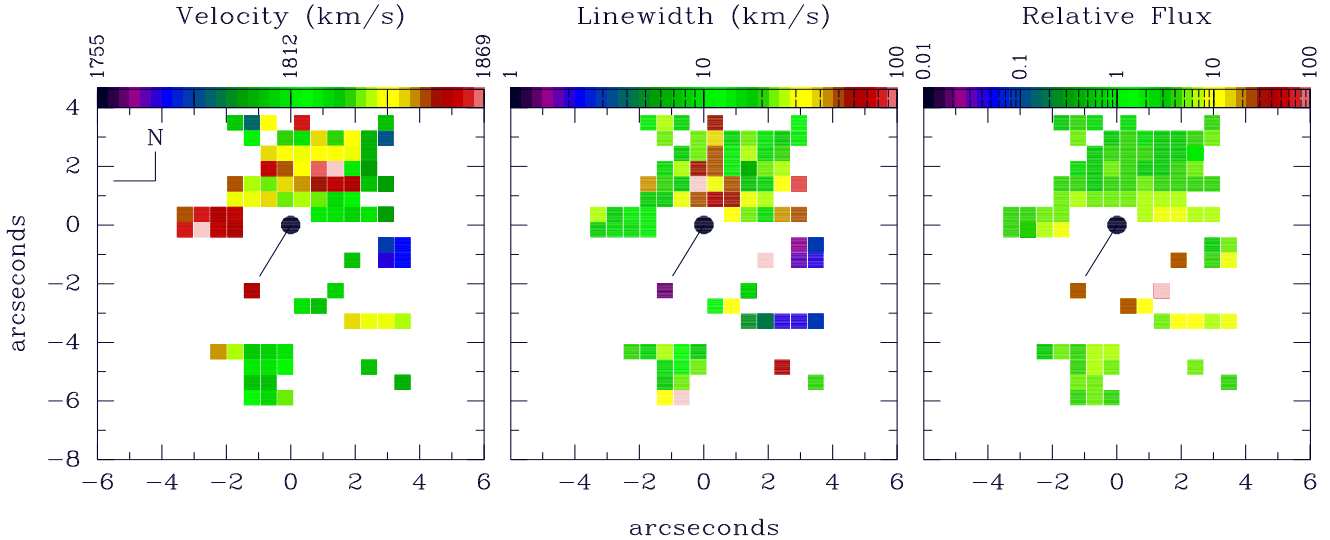


FIG. 3.— Velocities (left), widths (center) and fluxes (relative to Figure 2; right) of the second, broader component (component B). No rotation is apparent and no structure is apparent in either the width or flux fields.

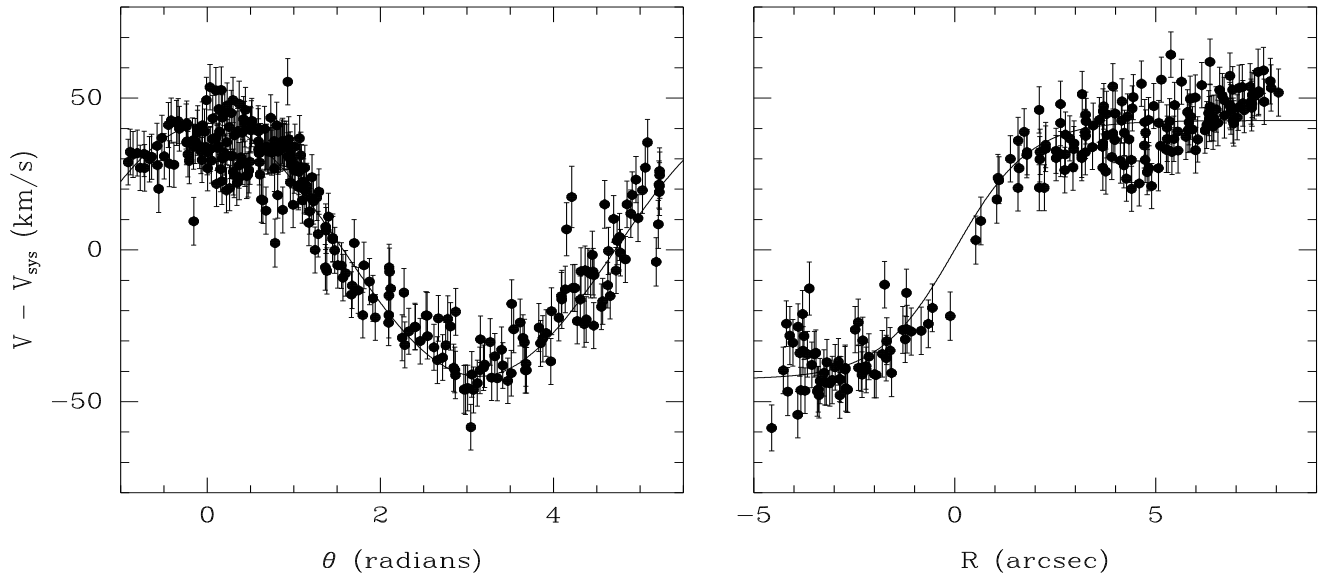


FIG. 4.— Measured velocities versus  $\theta$ , the de-projected azimuthal angle (left) and  $R$ , the de-projected radius (right) for an inclination of 25 degrees. In the rotation curve on the right, only velocities measured within  $60^\circ$  of the major axis are included. All velocity measurements on this rotation curve are projected onto the major axis by multiplying by  $\sec(\theta)$ . Error bars on velocities reflect the quadrature sum of the three terms included in equation 2: centroid measurement errors,  $\sigma_{\text{mod}}$ , and a beam-smearing contribution.

tion in the fit. The inclination derived from inverting the Tully-Fischer relation (Rix & Zaritsky 1995) falls between  $25^\circ$  and  $40^\circ$ . Therefore, we fit the velocity field with fixed inclinations varying between 5 and 50 degrees, normalizing the reduced- $\chi^2_\delta$  to unity (within 1%) by choosing an appropriate value of  $\sigma_{\text{mod}}$ . We found a major axis position angle of  $150^\circ \pm 1^\circ$ , an observed rotation velocity of  $V_{\text{rot}} = 44 \pm 2$  km/s, a heliocentric systemic velocity  $V_{\text{sys}} = 1793 \pm 1$  km/s, and a scale length  $h_{\text{rot}} = 1.8'' \pm 0.2''$  ( $\sim 200 \pm 20$  pc). The error on the kinematic center was just  $0.15''$  ( $\sim 20$  pc). While  $\sigma_{\text{mod}}$  systematically varied as a function of inclination, the other kinematic parameters and their associated errors, especially the kinematic center, do not change significantly with respect to the fitting error.

The isovelocity contours are not bent strongly as in

classic disk galaxy “spider diagrams,” as evidenced by Figure 2. While this adds to the uncertainty on the exact location of the kinematic center along the North-East to South-West axis of the galaxy, the spacing between contours (tightly bunched near the best-fit center and increased space between isovelocity contours further out) implies that the kinematic center robustly lies close to the nominal minor axis (compare Figure 4).

The kinematic center is offset with respect to the peaks in  $\text{H}\alpha$  flux and, as we shall see in Section 4.2, from the central cluster as well. The high precision with which we determine the kinematic center from our velocity field fitting does not include possible sources of systematic uncertainty: (a) We extracted one  $\text{H}\alpha$  component from two that were at different velocities without being able to unambiguously identify a physical reason to do so. (b)

Considering only this one component used in our velocity field modeling, there is a kinematic asymmetry  $5''$  along the major axis which is not understood (Figure 2 and Section 4.2). If this was taken as an indication that the velocity field is not well ordered, it could be used to argue against the NC formation mechanism that requires the center to be a special place in these late-type galaxies.

On the other hand, the center we find is quite robust. Leaving out some of the more questionable data, removing the kinematically asymmetric data, and trying to force the code to produce a center at a different location by varying the initial fit parameters all fail to produce a significant shift in the model kinematic center; none of the kinematic parameters change more than the errors quoted above. So, assuming a simple rotation curve and velocity field model, we find that the best fit kinematic center is well-constrained which implies a single strong minimum in  $\chi^2$  space. Figure 4 shows the derived rotation velocities against de-projected azimuthal angle and radius. We recover the expected sinusoidal shape and s-shape respectively, indicating that our simple model for the velocity field does an adequate job of describing the data. Forcing the kinematic center away from the best fit location would significantly alter the shape of these plots.

Further supporting evidence for the accuracy and interpretation of the ARGUS velocity field comes from the HI recession velocity: at first glance, the kinematic parameters derived from the  $H\alpha$  velocity field do not agree with the HI observations. In particular the  $H\alpha$ -derived systemic velocity ( $1793 \pm 1$  km/s) is much smaller than the value  $1837$  km/s found from HIPASS. While global line profile asymmetries can create differences between HI single dish recession velocities and the systemic velocities derived from velocity fields (Andersen & Bershadsky 2008), the sense of the discrepancy is reversed. The true systemic velocity, based on the asymmetry of the HI profile, should be even higher than  $1837$  km/s. However, as mentioned in Section 2, the Condon et al. (1996) radio continuum maps suggest that there are two discrete sources of radio emission from NGC 2139. If the stronger peak in the HI profile corresponds to the larger source of radio continuum emission associated with the main body of NGC 2139, then we find good agreement between this peak velocity ( $\sim 1795$  km/s) and our result. Furthermore, if the HI emission is coming from two distinct sources at two distinct velocities, then our measured rotation velocity will account for almost the whole width of the primary peak. Even if this “two gas clouds” picture is not correct, we are observing a sizable amount of the total rotation in NGC 2139 ( $44$  km/s from our  $H\alpha$  velocity field versus  $94$  km/s from the double-peaked HI profile) in a very small area near the center of the galaxy, lending credence to our interpretation that the kinematic center lies in the ARGUS field of view.

Finally, the velocity field possibly indicates that the luminous band described in Section 2 may be a star formation filament rather than a stellar bar because, as we show in the next section, the star formation knots are indeed located in this band, but the velocity field is not distorted by this feature. The kinematic center of NGC 2139 is well-separated from this band, and while bars are observed offset from galaxy centers in late-type galaxies, such as the LMC (de Vaucouleurs & Freeman 1972), this

behavior is often attributed to tidal forces (e.g., between the Milky Way and the LMC; van der Marel et al. 2002). Observations provide some evidence that NGC 2139 is affected by tidal forces, but whether the possible tidal effects are quantitatively sufficient to explain the offset we see between the stellar and gas kinematics is beyond the scope of this paper. Although we note that the distortions we observe in the velocity field seem unlike those expected from a bar (Roberts, Huntley & van Albada 1979), a separate study would be needed to convincingly argue against the presence of such a bar.

#### 4.2. IFU continuum to HST Image Registration

Before we can compare our best fit kinematic center to the location of the central cluster in NGC 2139, we need to register the HST WFPC2 F814W image of Boeker et al. (2002) to the continuum flux from the ARGUS IFU. We first measured continuum levels from the IFU data within a  $400 \text{ \AA}$  spectral window between  $6600 \text{ \AA} < \lambda < 7000 \text{ \AA}$  in which emission lines were masked.

We registered this continuum IFU image to the HST image by first smoothing the HST image with a  $0.8''$  Gaussian to roughly match the seeing during our ARGUS observations. Then, for a given position of the IFU with respect to the smoothed image, we extracted the flux within the footprint of each IFU spaxel. We fit a linear relation between the IFU and the HST spaxel fluxes and tabulated  $\chi^2$ . We mapped  $\chi^2$  over a grid in North-South and East-West offsets of the IFU with respect to the HST image, and found a very good fit between the HST extracted fluxes and IFU continuum fluxes. We used our  $\chi^2$  map to generate errors on our image to IFU registration (Figure 5).

With the IFU registered to the HST image, we can assign coordinates to the best fit kinematic center. This kinematic center is located at  $RA = 06^h 01^m 07.98^s$  and  $DEC = -23^\circ 40' 19.3''$  (J2000) with errors of  $\sim 0.2''$  on each axis (based on both registration errors and the formal velocity field errors). This is  $2.8''$  away from the location of the central cluster at  $RA = 06^h 01^m 07.88^s$  and  $DEC = -23^\circ 40' 21.7''$  (Figure 6). Here and hereafter all (RA, DEC) values refer to the J2000 coordinate system of the WFPC2 F814W HST image, which has an absolute accuracy with respect to the ICRS system of  $\sim 1''$ .

We note that the central cluster is coincident with a region poorly fit by the global velocity field (Figure 6), although the largest deviation from the velocity field does not correspond to any feature in the image. We also find that the central cluster is located near, but is not coincident with, the two peaks in  $H\alpha$  flux. The central cluster is separated by  $3.2''$  from the brightest source of  $H\alpha$  emission. This brighter, primary peak of  $H\alpha$  emission has no clearly identifiable counterpart in the HST I-band image. We postulate that the primary peak in  $H\alpha$  emission represents an even younger SSC perhaps still enshrouded in its birth-cloud. Perhaps future mid-infrared observations could reveal structures coincident with the large deviation from the velocity field South-West of the central cluster and the bright peak in  $H\alpha$  emission to its West.

#### 4.3. Determination of the Photometric Center

Finally, we re-determine the location of the photometric center of NGC 2139 from the HST WFPC2 F814W

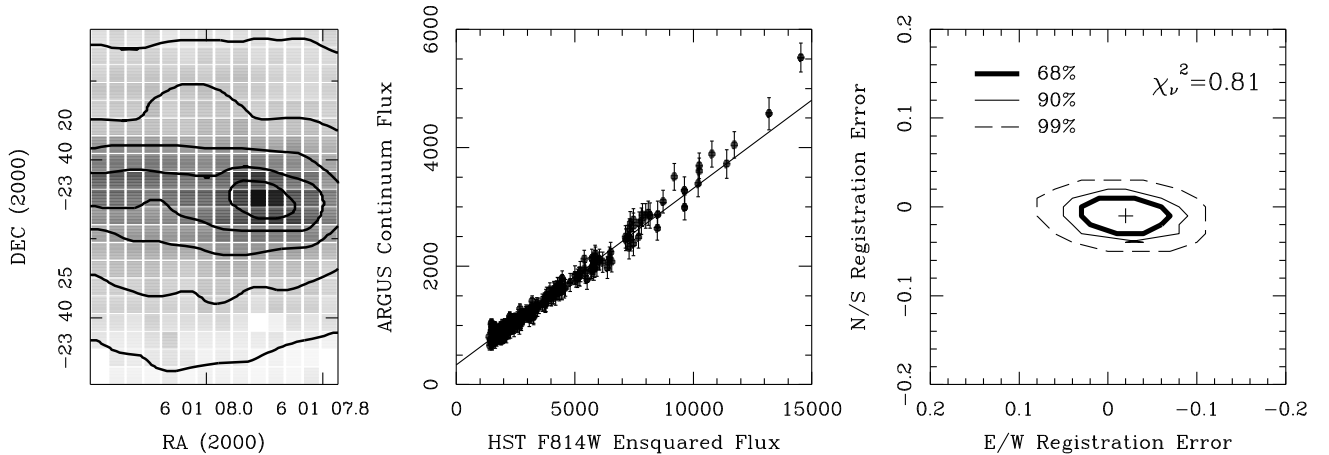


FIG. 5.— Left Panel: continuum levels from VLT ARGUS spaxels overlaid with smoothed (by  $0.8''$ ) HST image contours of the center of NGC 2139 at the best-fit registered position. Center Panel: spaxel-ensquared HST WFPC2 F814W flux versus ARGUS continuum flux with best fit linear regression. Right Panel: error contours of the image to IFU registration based on the  $\chi^2$  map. The reduced  $\chi^2$ ,  $\chi_\nu^2$ , for the fit was 0.81, indicating a good fit.

image. This exercise had been carried out in Böker et al. (2002) with the aim to derive photometric centers for a large number of galaxies in a homogeneous way. Here we focus on understanding one special case. Indeed, NGC 2139 has a rather irregular appearance on the PC chip. In particular, the luminous band going through the center of the object has a number of secondary brightness peaks (secondary to the central cluster), which have the effect to shift the photocenter each time the radius of the isophotal ellipse becomes large enough to include one more of these peaks. We have therefore convolved the image with a  $\sigma = 10''$  Gaussian before using the exact same setup as Böker et al. (2002). We now define the isophotal center to be the arithmetic mean of all ellipse centers between radii of  $0.7''$  and  $18.4''$ . We thus obtain the following photocenter: RA =  $06^h 01^m 07.95^s \pm 0.09^s$  and DEC =  $-23^\circ 40' 21.6'' \pm 0.4''^3$ . The photometric center is  $2.3'' \pm 1.4''$  away from the kinematic center and  $1.0'' \pm 1.4''$  away from the central cluster. We note that this result still depends strongly on the range of radii used to determine the photometric center. The location of the photometric center is shown in Figure 6.

##### 5. NUCLEAR CLUSTER OR YOUNG SUPER STAR CLUSTER?

We have provided new data to judge whether the classification of the central star cluster in NGC 2139 as a NC is correct. While all the results we have obtained from the H $\alpha$  velocity field are consistent with the interpretation of the cluster being a nascent NC, we examine here the possibility that this cluster is not a NC and instead is a more normal young super star cluster (SSC). This is supported by the emission line profiles as observed in the VLT/UVES data published in Walcher et al. (2005, 2006). Figure 7 shows the [S II] doublet emission lines in 3 apertures along the spatial direction. It is clear that the lines are broadest at the location of the central cluster. The FWHM for this aperture, as determined from a single Gaussian fit is  $2.3 \text{ \AA} = 100 \text{ km/s}$ . However, the lines have two separate kinematic components, consistent with the ARGUS H $\alpha$  data. These two components

can be fit by two Gaussians, but high-velocity wings remain that are not fit even by this 2-Gaussian fit. These wings have a full width at zero intensity of 300 km/s. The redder peak is coincident in velocity with the cluster stars (measured from the Ca Triplet), while the bluer peak is separated by approximately 55 km/s. One could speculate that we are seeing a super-bubble around the cluster, where the part that is coming towards us is visible, while the receding part of the bubble is hidden by extinction inside the cluster itself. Such complex emission lines with two components are routinely seen in HII regions and very young clusters (e.g. Vanzì et al. 2006, Henry et al. 2007).

The stellar velocity dispersion for the cluster in NGC 2139 is  $\sigma_* = 16.5 \pm 1 \text{ km/s}$  (Walcher et al. 2005). So its escape velocity is approximately  $\sqrt{2}\sigma_* \approx 23 \text{ km/s}$ . This means that the gas in the peak coincident with the cluster is marginally bound ( $\sigma_{\text{gas}} = 20 \text{ km/s}$ ). However, neither the high-velocity wings, nor the gas moving towards us are bound to the central cluster.

These properties can be compared to the discussion in Gilbert & Graham (2007). These authors publish emission line widths for a large sample of SSCs in the Antennae. The velocities in the NGC 2139 cluster are consistent with, yet at the high end, of those observed by Gilbert & Graham. As these authors show, such high velocities and complex line profiles are associated with winds and mass loss from very young star clusters, so-called SSCs. Naturally, star formation and winds could also be associated with a NC undergoing a rejuvenation burst.

We also remind the reader that the effective radius of the NGC 2139 cluster is 10pc and is one of the largest in the Böker et al. (2004) sample. This could be interpreted in the context of the study of Mengel et al. (2005), who show that the radii of SSCs are linked to their age. These authors show that the effective radii of typical SSCs are  $16 \pm 15 \text{ pc}$  for 4 Myr old clusters and  $6.5 \pm 5.3 \text{ pc}$  for 8-11 Myr old clusters. In Gilbert & Graham these large radii are interpreted as expansion following mass-loss through winds. Of course, a similar effect could puff up the radius of young NCs when compared to their older cousins.

The environment around the central star cluster also

<sup>3</sup> The photometric center determined from the DSS image of NGC 2139 was statistically equivalent.

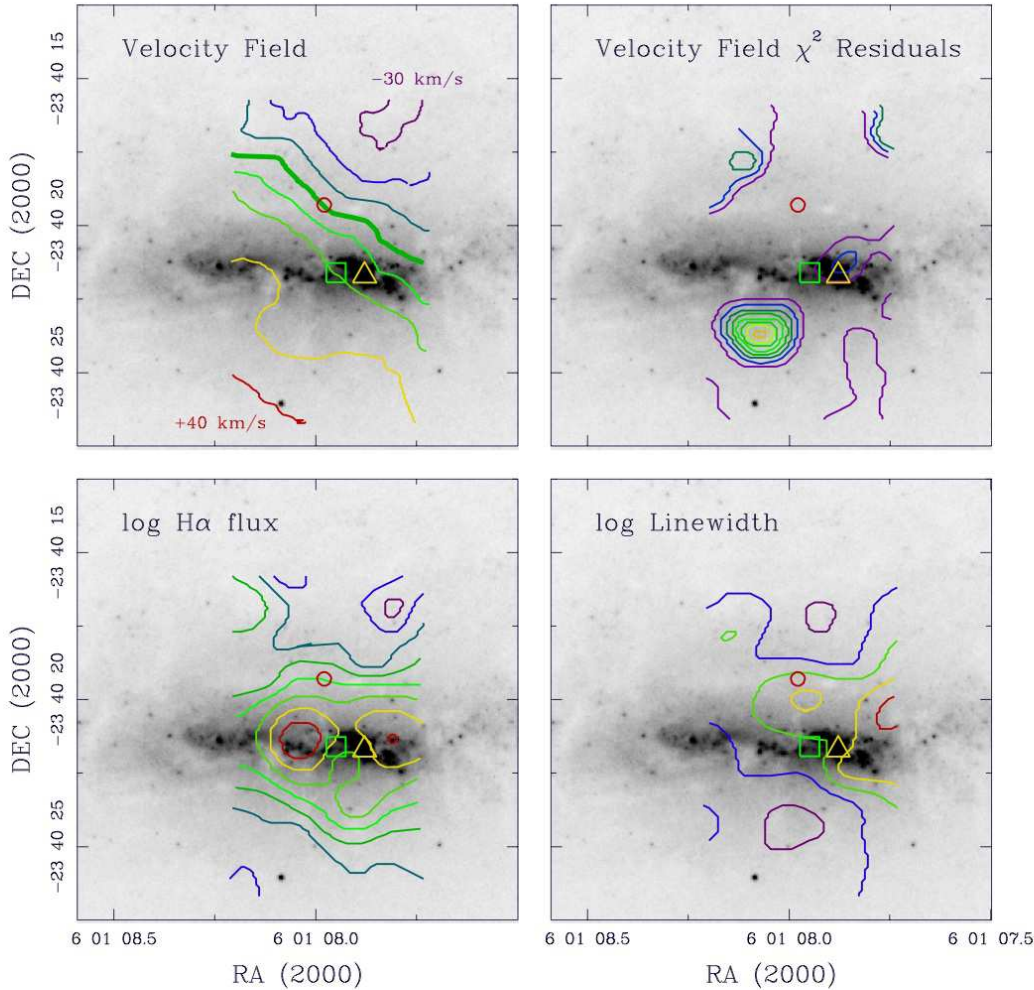


FIG. 6.— Upper Left Panel:  $H\alpha$  isovelocity contours for the central regions of NGC 2139 overlaid on the HST WFPC2 F814W image. In all plots of this figure, the red circle marks the location of the kinematic center, the green box marks the location of the photometric center, and the triangle marks the location of the central cluster. All coordinates refer to those of the HST image. IsovLOCITY contours are separated by 10 km/s, with the extreme velocities listed with respect to the systemic velocity. Upper Right Panel:  $\chi^2$  contribution to the velocity field best-fit kinematic model. Different colors are separated by  $\Delta\chi^2 = 1$ , from  $\chi^2 = 1$  (purple) to 8 (red). The large kinematic asymmetry  $5''$  from the kinematic center is the dominant feature and does not appear to be associated with any feature in the HST image. A second significant kinematic asymmetry is apparent, coincident with the central cluster. Lower Left Panel:  $H\alpha$  flux level contours (see Figure 2 for relative values of the fluxes) overlaid on the HST image. Two strong peaks on star formation are apparent. Neither is coincident with the central star cluster. In general, the luminous band has higher  $H\alpha$  fluxes than the regions outside. Lower Right Panel:  $H\alpha$  linewidth contours overlaid on the HST image. Each contour is separated by steps of 0.15 in log linewidth from  $10^{1.05} = 11.2$  km/s (red) to  $10^{0.45} = 2.8$  km/s (violet). While the linewidths are slightly larger near the star cluster and within the luminous band, we do not see a clear correspondence between the linewidths and any of the other mapped quantities.

suggests that this may be one of multiple SSCs in NGC 2139. The multiple sources of radio continuum emission, the luminous band in which the central star cluster is located, the larger-scale tidal features and the multi-component  $H\alpha$  and [S II] emission all are consistent with a recent merger event, which may drive gas to the center and initiate the formation of SSCs. Indeed, the two bright  $H\alpha$  sources in the vicinity of the central star cluster may be very young SSCs.

While the above arguments lead to a certain degree of uncertainty with regards to the classification of the central cluster in NGC 2139, we can predict whether we would identify the cluster 3 Gyr from now as a NC. Using a mass-to-light ratio  $M/L_I = 0.87$ , as predicted by and

model predictions from Bruzual & Charlot (2003) for a 3 Gyr old stellar population and using a cluster mass of  $8 \times 10^5 M_\odot$ , we obtain  $L \approx 7 \times 10^5 L_\odot$  after 3 Gyr. This is significantly brighter than the cutoff luminosity of a NC as observed in Böker et al. (2002)<sup>4</sup>.

If the identified central star cluster can somehow merge with other nearby clusters (such as those associated with the two bright peaks of star formation in the  $H\alpha$  map) and fall to the kinematic center, then the resultant NC could be even brighter. If this were to happen, this

<sup>4</sup> No NC with a luminosity below  $M_I = -9$  was detected, despite sufficient sensitivity. Using  $M_I = -2.5 \log(L_I) + 4.08$  this corresponds to  $2 \times 10^5 L_\odot$ .



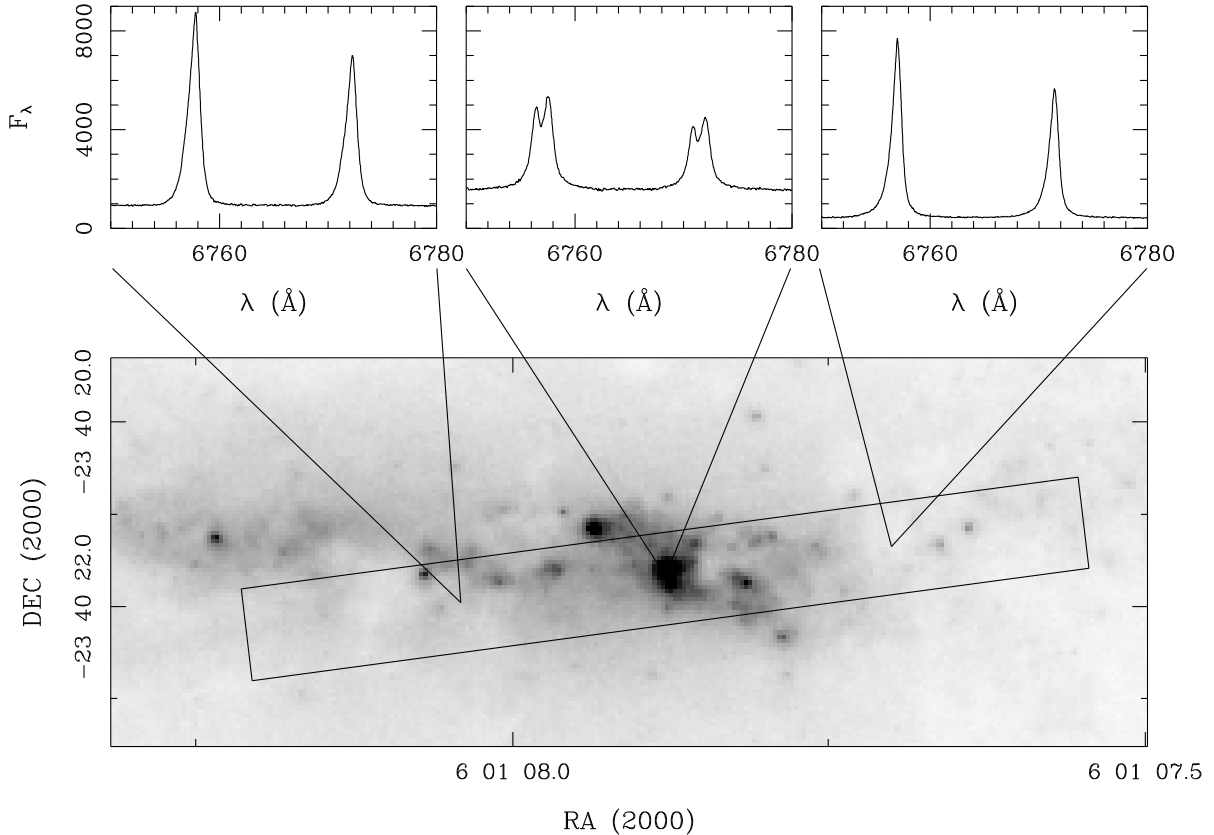


FIG. 7.— Top Panels: the spatial profiles of the [S II] emission lines measured from VLT/UVES high resolution spectra ( $R \sim 30000$ ) in three apertures of  $1'' \times 1''$ . One aperture includes the central cluster itself and one aperture 2 arcseconds on either side are also shown. Bottom Panel: HST WFPC2 F814W image centered on the central star cluster of NGC 2139 with the UVES slit overlaid. The broad emission lines in general and the double peaked emission line on the central cluster in particular are compatible with a very young massive star cluster (SSC) in a region actively forming stars.

would support the NC formation scenario whereby multiple stellar clusters coalesce to form the final NC (Fellhauer et al. 2002). That so many young clusters are present near the center of NGC 2139 is another indication that the galaxy recently experienced a tidal interaction capable of forming clusters (Bekki et al. 2004).

We now assess the probability that such a massive and luminous cluster would form by chance in a late-type disc galaxy such as NGC 2139. To that end, we compute the star formation rate (SFR) necessary to produce a cluster of mass similar to the central cluster in NGC 2139. Due to size of sample effect, the maximum mass  $M_{max}$  of a star cluster scales with the total number  $N$  of star clusters formed, or equivalently with the star formation rate (see Larsen, 2002). The central cluster in NGC 2139 has an absolute I-band magnitude of  $M_I = -12.65$  (Böker et al. 2002) and from its age and Bruzual & Charlot (2003) we infer a colour  $V-I = 0.5$ . Following the relations given in Weidner et al. (2004), we infer that a total SFR of roughly  $1 M_{\odot}/\text{yr}$  is needed to form one such cluster. Emission line fluxes for NGC 2139 are given in Moustakas & Kennicutt (2006) for a nuclear aperture of  $2.5'' \times 2.5''$  and the total galaxy ( $120'' \times 120''$ ). The  $H\alpha$  fluxes are  $23.11 \pm 0.97 \times 10^{-15} \text{ ergs s}^{-1} \text{ cm}^{-2}$  and  $3310 \pm 130 \times 10^{-15} \text{ ergs s}^{-1} \text{ cm}^{-2}$  respectively. Using a distance of 23.6 Mpc (Böker et al. 2002) and the standard Kennicutt (1998) conversion of  $\text{SFR} [M_{\odot}/\text{yr}] = 7.9 \times 10^{-42} L_{H\alpha} [\text{erg/s}]$ , we obtain nuclear and total SFRs

of 0.01 and  $1.7 M_{\odot}/\text{yr}$ , respectively. The central cluster is the brightest cluster in the area of the PC chip, which is  $36'' \times 36''$  ( $4\text{kpc} \times 4\text{kpc}$ ). However, the surface brightness of the galaxy falls rapidly outside of the chip, so it is likely that most of the  $H\alpha$  flux observed by Moustakas & Kennicutt stems from the actually observed area. In summary, it is likely that a cluster similar to the one observed in NGC 2139 forms somewhere in the disk of the galaxy. The likelihood that this happened by chance in the central  $2.5'' \times 2.5''$  however remains low. Note though, that with the 40 km/s current rotational speed of the galaxy and the estimated cluster age, the cluster could have moved by as much as 1.5 kpc since formation. As the cluster seems to have formed from disk material and is still associated with the gas overdensity in which it formed, it is not likely, however, that the cluster has a large peculiar motion with respect to the rest of the galaxy disk. Whether special conditions close to the center of the galaxy need to be invoked thus remains open.

## 6. SUMMARY

We have presented VLT/ARGUS IFU data to ascertain whether the location of the kinematic center of the late-type galaxy NGC 2139 and the location of its central cluster, previously classified as a NC, coincide spatially. We have analyzed the velocity field in the ARGUS field of view and found the kinematic center to be

at  $06^h01^m07.98^s$  and  $\text{DEC} = -23^\circ40'19.3''$  with errors of  $\sim 0.2''$  on each axis. The location of the central cluster is at  $\text{RA} = 06^h01^m07.88^s$  and  $\text{DEC} = -23^\circ40'21.7''$ ,  $2.8''$  offset from the kinematic center. The photometric center is at  $\text{RA} = 06^h01^m07.95^s \pm 0.09$  and  $\text{DEC} = -23^\circ40'21.6'' \pm 0.4''$  and is  $2.3'' \pm 1.4''$  away from the kinematic center and  $1.0'' \pm 1.4''$  away from the central cluster. While some caveats remain concerning the precision which we quote for the location of the kinematic center, it appears unlikely that the location of the NGC 2139 central star cluster is coincident with the kinematic center.

Based on the peculiar  $\text{H}\alpha$  and [S II] emission from the core of NGC 2139, we conclude that the central cluster is actively forming stars. While the properties of the central cluster in NGC 2139 are thus compatible with those of a SSC, we have presented several arguments why it can nonetheless be considered to be a NC progenitor object:

- Based on the projected luminosity of the cluster in 3 Gyr, it would be classified as a NC in the survey of Böker et al. (2002), if the cluster does not lose a significant fraction of its mass due to evaporation.
- Other young star clusters associated with peaks in the  $\text{H}\alpha$  distribution may merge with the visible one to produce a multi-aged, very luminous NC. Alternatively, more gas from the luminous band may fall into the central star cluster and form stars in situ.
- While the NGC 2139 central cluster is not presently at the center, the relatively well-ordered velocity field means that the cluster should fall to the center within a relatively short period of time: if the cluster is 320pc ( $2.8''$ ) away from the kinematic center with a rotation velocity of 15 km/s, Equation 1 yields a derived dynamical friction timescale of 110 Myr, comfortably longer than the age of 41 Myr derived by Walcher et al. (2006). It should be noted, however, that this is only an order of magnitude estimation as it will depend on the ex-

act form of the gravitational potential. In the case considered by Milosavljević (2004), the value we derive is a lower bound. On the other hand, if NGC 2139 is undergoing a dissipative tidal interaction, as the images and radio data seem to indicate, then the dynamical friction timescale for the central star cluster could be significantly shorter (e.g. Peñarrubia, Just & Kroupa 2004; Capuzzo-Docetta & Vicari 2005; Miocchi et al. 2006; Fujii et al. 2007). Regardless, it appears that within a relatively short time this cluster may take up residence at the nucleus of NGC 2139.

Although we caution that NGC 2139 is in many ways an unusual object among all late-type spirals containing NCs, we can attempt to view our results in terms of the three hypotheses described in Section 1. We find a confusing picture: the properties of the central cluster in NGC 2139 are compatible with the free-roaming seed cluster formation hypothesis (2). However, we observe clear rotation of the galaxy, which is as predicted by scenario (1). Finally, a second cluster seems to be forming close to the visible central cluster suggesting that for NCs the merger mechanism described in scenario (3) can also play a role.

In summary, it appears that seed NCs have been formed in NGC 2139, fed by an inflow of gas, possibly due to a recent merger event. It is clear that larger datasets will be needed to clarify whether NCs in general are true galaxy nuclei. IFUs with larger FOVs would help in this endeavor, particularly if the central velocity fields are more disordered than that observed in NGC 2139. The field would also enormously benefit from targeted simulations assessing the viability of the three formation scenarios in relation to all the observed properties of NCs.

#### ACKNOWLEDGMENTS

CJW is supported by the MAGPOP Marie Curie EU Research and Training Network. JS thanks Andrea Gilbert for informative conversations regarding SSCs.

#### REFERENCES

- Andersen, D.R., Bershad, M.A., Sparke, L.S., Gallagher, J.S. & Wilcots, E.M. 2001, *ApJ*, 551, L131  
 Andersen, D.R., et al. 2006, *ApJS*, 166 505  
 Andersen, D.R. & Bershad, M.A. 2007, *submitted to ApJ*  
 Balcells, M., Graham, A.W., Domnguez-Palmero, L., Peletier, R.F. 2003 *ApJ* 582 79  
 Bekki, K., et al. 2004, *ApJ*, 610, L93  
 Böker, T., et al. 1999, *ApJS*, 124, 95  
 Böker, T., Laine, S., van der Marel, R.P., Sarzi, M., Rix, H.-W., Ho, L.C., Shields, J.C. 2002, *AJ*, 123, 1389  
 Böker, T., Sarzi, M., McLaughlin, D.E., van der Marel, R.P., Rix, H.-W., Ho, L.C., Shields, J.C. 2004, *AJ*, 127, 105  
 Bruzual, G., Charlot, S. 2003, *MNRAS*, 344, 1000  
 Capuzzo-Dolcetta, R. & Miocchi, P. 2008, *astro-ph/0801.1072*  
 Capuzzo-Dolcetta, R. & Vicari, A. 2005, *MNRAS*, 356, 899  
 Carollo, C.M., Stiavelli, M., Mack, J. 1998, *AJ*, 116, 68  
 Chandrasekhar, S. 1943, *ApJ*, 97, 255  
 Condon, J.J., Helou, G., Sanders, D.B., Soifer, B.T. 1996, *ApJS*, 103, 81  
 Côté, P., et al. 2006, *ApJS*, 165, 57  
 de Blok, W.J.G., Bosma, A., & McGaugh, S.S. 2003, *MNRAS*, 340, 657 1997, *AJ*, 114, 1858  
 de Blok, W.J.G. 2005, *ApJ*, 634, 227  
 de Vaucouleurs, G., de Vaucouleurs, A., Corwin, H.G., Jr., Buta, R.J., Paturel, G., Fouque, P. 1991, in “Third Reference Catalogue of Bright Galaxies”, Springer  
 de Vaucouleurs, G. & Freeman, K.C. 1972, *Vistas in Astronomy*, 14, 163  
 Emsellem, E. & van de Ven, G. 2008, *ApJ*, 674, 653  
 Fellhauer M., Baumgardt H., Kroupa P., Spurzem R., 2002, *Cel. Mech. Dyn. Astron.*, 82, 113  
 Ferrarese, L., & Merritt, D. 2000, *ApJ*, 539, 9  
 Ferrarese, L., 2002, *ApJ*, 578, 90  
 Filippenko, A. V., & Ho, L. C. 2003, *ApJ*, 588, L13  
 Fujii, M., Iwasawa, M., Funato, Y, Makino, J. 2007, *arXiv* 0708.3719  
 Gebhardt, K., et al. 2000, *ApJ*, 539, L13  
 Gilbert A.M., Graham, J.R. 2007, *arXiv* 0706.3935, accepted by *ApJ*  
 Graham, A.W., Erwin, P., Caon, N., Trujillo, I. 2001, *ApJ*, 563, L11  
 Häring, N., Rix, H.-W. 2004, *ApJ*, 604, L89  
 Henry, A.L., Turner, J.L., Beck, S.C., Crosthwaite, L.P., Meier, D.S. 2007, *AJ*, 133, 757  
 Kennicutt, R.C. 1998, *ARA&A*, 36, 189  
 Koribalski, B.S., et al. 2004, *AJ*, 128, 16  
 Larsen, S.S. 2002, *AJ*, 124, 1393

- Magorrian, J., et al. 1998, *AJ*, 115, 2285
- Matthews, L.D., et al. 1999, *AJ*, 118, 208
- Mengel, S., Lehnert, M.D., Thatte, N., Genzel, R. 2005, *A&A*, 443, 41
- Milosavljević, M., 2004, *ApJ*, 605, L13
- Miocchi, P., Capuzzo-Dolcetta, R., Di Matteo, P., Vicari, A. 2006, *ApJ*, 644, 940
- Moustakas, J. & Kennicutt R.C. 2006, *ApJS*, 164, 81
- Oh, K.S. & Lin, D.N.C. 2000, *ApJ*, 543, 620
- Paturel, G., et al. 2003, *A&A*, 412, 45
- Peñarrubia, J., Just, A., Kroupa, P. 2004, *MNRAS*, 349, 747
- Phillips, A.C., Illingworth, G.D., MacKenty, J.W., Franx, M. 1996, *AJ*, 111, 1566
- Rix, H.-W., Guhathakurta, P., Colless, M., Ing, K. 1997, *MNRAS*, 285, 779
- Rix, H.-W. & Zaritsky, D. 1995, *ApJ*, 447, 82
- Roberts, W.W., Huntley, J.M., & van Albada, G.D. 1979, *ApJ*, 233, 67
- Rossa, J., van der Marel, R.P., Böker, T., Gerssen, J., Ho, L.C., Rix, H.-W., Shields, J.C., Walcher, C.-J. 2006, *AJ*, 132, 1074
- Scarlata, C. et al. 2004 *AJ*, 128, 1124
- Seth, A.C., Dalcanton, J.J., Hodge, P.W., Debattista, V.P. 2006, *AJ*, 132, 2539
- Shields, J.C., et al. 2008 *ApJ*, in press
- Valenzuela, O., Rhee, G., Klypin, A., Governato, F., Stinson, G., Quinn, T., Wadsley, J. 2007, *ApJ*, 657, 773
- Van der Marel, R.P., Alves, D. R., Hardy, E. Suntzeff, N. B. 2002, *AJ*, 124, 2639
- Vanzi, L., Scatarzi, A., Maiolino, R., Sterzik, M. 2006, *A&A*, 459, 769
- Walcher, C.J., van der Marel, R.P., McLaughlin, D., Rix, H.-W., Böker, T., Häring, N., Ho, L.C., Sarzi, M., & Shields, J.C. 2005, *ApJ*, 618, 237
- Walcher, C.J., Böker, T., Charlot, S., Ho, L.C., Rix, H.-W., Rossa, J., Shields, J.C., van der Marel, R.P. 2006, *ApJ*, 649, 692
- Weidner, C., Kroupa, P., Larsen, S.S. 2004, *MNRAS*, 350, 1503